

Wintertime radiation and energy budget along an urbanization gradient in Montreal, Canada

Onil Bergeron and Ian B. Strachan*

Department of Natural Resource Sciences, McGill University, Ste. Anne de Bellevue, QC, Canada

ABSTRACT: This study reports on the radiation and energy balance of three sites (rural, suburban, and urban) located along an urbanization gradient in the Montreal, QC, region for two winters (December–March) with contrasting snow regimes. The urban and suburban sites had similar albedo which was about half that at the rural site during the snow-cover period. Temporal variability in albedo was attributable to the presence of snow on rooftops at the urban site and to a site-specific response to cloudiness at the suburban site. As compared to the suburban site, the urban site showed higher albedo inducing lower net radiation (Q^*) which was compensated for by greater anthropogenic heat flux (Q_F), so that the urban site had highest total available energy ($Q^* + Q_F$). Hourly Q_F estimates were a significant term in the winter energy budget analysis. Q_F was dominated by building heating at both urbanized sites, while vehicular traffic contributed to rush hour peaks. Daytime total available energy was mostly dissipated as sensible heat flux (Q_H) at the beginning of the winter season and mostly stored (ΔQ_S) towards the end of the winter at both urbanized sites. Daytime energy partitioning into Q_H and ΔQ_S was correlated with air temperature with no significant differences between urbanized sites. On a daily time scale, available energy was mostly stored before noon and dissipated as Q_H in the afternoon at both urbanized sites. Urbanized sites showed differences in diurnal variability of Q_H and ΔQ_S occurring in the afternoon and evening. Latent heat flux (Q_E) was low throughout winter and accounted for 10% of the total available energy during daytime at the urbanized sites. Water vapour emissions showed intra-urban differences in their response to wintertime climatic conditions. Copyright © 2010 Royal Meteorological Society

KEY WORDS urban climate; energy budget; anthropogenic heat flux; wintertime; snow; albedo; Montreal; eddy covariance

Received 5 February 2010; Revised 27 September 2010; Accepted 2 October 2010

1. Introduction

The world's population is increasingly urbanized and currently about 80% of the Canadian population lives in cities. Characteristics of urban fabrics, structure, and orientation can influence the properties of the near-surface atmosphere over cities and local climates. Understanding the interaction between the energy balance and the urban surface characteristics is therefore crucial. Simultaneously, computational power has been growing, allowing meso-scale models to run at higher resolution, thus enabling the incorporation of detailed surface characteristics, including urban features, in weather prediction schemes. However, weather forecasting abilities over cities are inadequate because of current limitations of surface process models and to a restricted number of observational studies available in the literature.

The Environmental Prediction in Canadian Cities (EPICC) Research Network (www.epicc.uwo.ca) was created to serve a threefold purpose: (1) report observations of energy balance components using (eddy covariance) flux towers for two Canadian cities with contrasting

climates; (2) quantify each site's surface characteristics using remote sensing; and (3) test and couple the urban surface parameterization scheme TEB (Masson, 2000) to the SVAT model ISBA (Noilhan and Planton, 1989) to be ultimately implemented into the Canadian weather modelling and prediction system. The cities of Montreal and Vancouver were selected to allow an emphasis on winter snow and summer irrigation, respectively. This study focuses on observations made in Montreal during the winters of 2007–2008 and 2008–2009 which experienced contrasting snow regimes.

There are a number of studies reporting on wintertime urban energy budget with varying degrees of detail (Grimmond, 1992; Ruffieux, 1995; Spronken-Smith, 2002; Christen and Vogt, 2004; Offerle *et al.*, 2005, 2006; Spronken-Smith *et al.*, 2006; Coutts *et al.*, 2007; Lemonsu *et al.*, 2008; Pigeon *et al.*, 2008; Vesala *et al.*, 2008; Leroyer *et al.*, 2010). However, studies on the role of snow on urban energy budget at the neighbourhood level are rare. Lemonsu *et al.* (2008) and Leroyer *et al.* (2010) showed that snow can influence energy flux partitioning during discrete snowmelt periods in Montreal; this study represents an opportunity to extend their findings to the entire wintertime period for two years under different snow regimes.

* Correspondence to: Ian B. Strachan, Department of Natural Resource Sciences, McGill University, Macdonald Campus, 21,111 Lakeshore Road, Ste. Anne de Bellevue, QC H9X 3V9, Canada.
 E-mail: ian.strachan@mcgill.ca

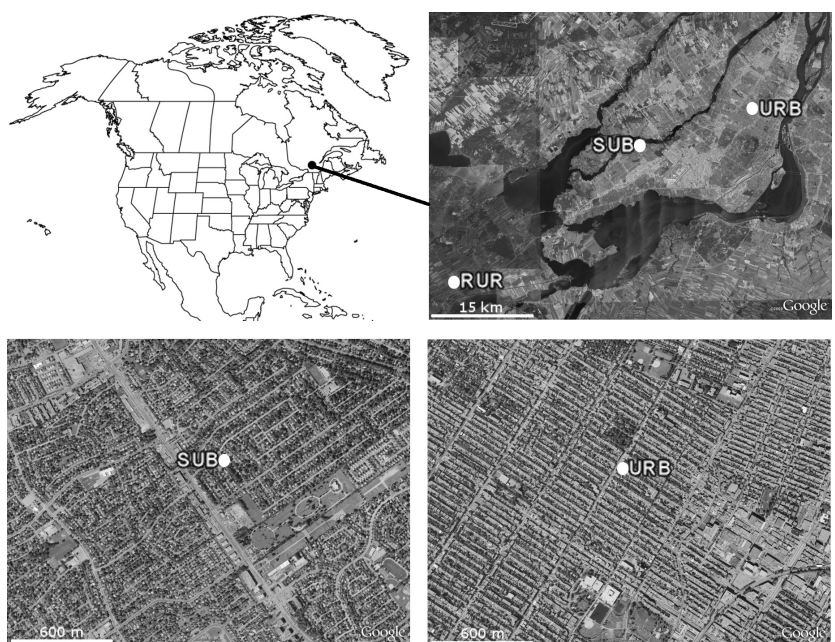


Figure 1. Aerial photographs of the suburban (SUB) and urban (URB) sites. North is towards the top of the figure. Images from www.worldatlas.com and Google Earth[®].

In urban flux tower studies, anthropogenic heat flux estimates are usually overlooked or are deduced from other energy balance terms. Hence, the reported energy budgets are somewhat incomplete and may lump together the variability of different components into one residual term. Sailor and Lu (2004) proposed a simple methodology to estimate the within-day anthropogenic heat flux using information from energy consumption data, vehicular traffic, and population density at spatial scales ranging from neighbourhoods to cities or regions, a technique which is particularly suitable for flux tower studies. Their methodology has been adapted given the available data to provide hourly estimates of anthropogenic heat flux for urban and suburban areas in Montreal.

Our study focuses on characterizing the effect of urbanization on wintertime radiation and energy balance in the Montreal region. The specific objectives of this study were to (1) provide hourly estimates of anthropogenic heat loss at the spatial scale of the study sites (10^4 – 10^6 m 2) for inclusion in the energy balance; (2) describe the seasonal and diurnal variability of the radiation and energy balance components for two winters with contrasting snow regimes; and (3) determine key environmental factors or site characteristics that can help explain this variability.

2. Methods

2.1. Site description

Three flux towers were deployed in the region of Montreal, Canada, along an urbanization gradient that followed an east-to-west transect (Figure 1). Site characteristics are listed in Table I.

The urban site (URB) was located in the Rosemont-La-Patrie borough which is a densely populated (8400 inh. km $^{-2}$) residential area with two- or three-storey row housing which translated into well defined street canyons and alley canyons (Figure 1). Urban fabrics mostly include paved streets and alleys, gravel on flat rooftops, and brick walls. Backyards and frontyards are small with sparse vegetation (mostly grass, herbs, and shrubs) and are bordered with impervious materials (paved alley, sidewalk, parking lot, or building). Sheds or garages are present in most backyards. Single deciduous trees taller than the surrounding buildings are a regular feature in SE–NW-oriented street canyons. Opposing SW–NE-oriented streets include commercial and institutional activity. The Métropolitaine Highway is about 2 km NW of the flux tower site, while a 2.9 ha park and a 63 ha park are located 150 m N and 2.3 km NE, respectively.

The suburban site (SUB) was located about 18 km WSW of URB in the Pierrefonds-Roxboro borough, a single-family residential area (3150 inh. km $^{-2}$) with detached houses and well-defined street canyons (Figure 1). Swimming pools are common in backyards while sheds are few. rooftops are mostly sloped and covered with dark shingles. Exterior walls are bricks or vinyl siding. Grass, shrubs, and tall coniferous and deciduous trees are present in both backyards and frontyards. Commercial activity is present on one N-S major street located W of the flux tower. A 20 ha cemetery is found about 500 m SE of the flux tower site and the Des Prairies river flows 1.5 km N.

The rural site (RUR) was located in Coteau-du-Lac, Quebec, an agricultural area off the Island of Montreal about 35 and 50 km SW of SUB and URB, respectively, in the upwind direction (Figure 1). Sparse housing and farm buildings are present but were outside the flux

Table I. Site characteristics.

	URB	SUB	RUR ^a
Latitude, Longitude (°)	45.547 N, 73.592 W	45.501 N, 73.811 W	45.328 N, 74.165 W
Land use	Residential	Residential	Agricultural
Urban climate zone ^b	3	5	7
Population density (inh. km ⁻²)	8400 ^d	2400 (3150) ^e	—
z_H , mean building height (m) ^f	7.9	6.4	—
z_{TT} , mean tall tree height (m) ^c	13.0	13.8	—
z_M , measurement height (m)	25	25	2
W, mean street canyon width (m)	25.2	32.2	—
z_H/W , street aspect ratio	0.32	0.22	—
Roof materials	Gravel	Shingle	—
Roof orientation	Flat	2-facets 10–15° from horizontal	—
Exterior building wall materials	Brick	Brick or shingle	—
Surface cover fractions (%) ^f			
λ_I , impervious (pavement)	44	37	0
λ_P , built (roofs)	27	12	0
λ_V , vegetation (grass and trees)	29	50	100
Grass	3	30	100
Trees	26	20	0

^a Urbanization is assumed to be nil at RUR.^b Oke (2006).^c Includes only trees > z_H .^d 133 618 inh./15.9 km² (Ville de Montréal, 2009a).^e 65 041 inh./27.1 km² [65 041 inh./20.6 km² when three parks (201, 288, and 159 ha) are removed from borough surface area] (Ville de Montréal, 2009a, 2009b).^f Surface cover fractions and mean building heights estimated from Quickbird image, building, and GIS information for a 1000 m radius centred on the towers at SUB and URB (Jinfei Wang, personal communication). At SUB, 1% of the surface is classified as other (open water, swimming pools, or bareground).

source areas. The flux tower was deployed in a field which lay fallow during the winter periods.

2.2. Instrumentation

All flux towers were equipped with similar instrumentation that was cross-checked against each other before deployment. Each flux tower had an eddy covariance system mounted at z_M (Table I) that comprised a sonic anemometer–thermometer [model CSAT3, Campbell Scientific Canada Corp. (CSCC), Edmonton, AB, Canada] to measure three-dimensional wind components and air temperature as well as an infra-red gas analyzer (model LI-7500, Li-COR Biosciences, Lincoln, NE, USA) to measure H₂O concentration and atmospheric pressure. The eddy covariance system sampled at 20 Hz using a datalogger (models CR5000 at URB and SUB and CR1000 at RUR, CSCC) and raw data were stored for post-processing.

Supporting meteorological variables were sampled at 0.5 Hz and averaged on a 5-min basis using a datalogger (models CR23X at all sites and CR1000 for radiation data at RUR, CSCC). A non-heated, four-component radiometer (model CNR1, Kipp & Zonen, Delft, The Netherlands) was used to measure incoming shortwave (K_{in}) and longwave (L_{in}) radiation, outgoing shortwave (K_{out}) and longwave (L_{out}) radiation, albedo ($\alpha = K_{out}/K_{in}$), and net radiation (Q^*) at z_M . At URB, radiation measurements were made at the top of the flux tower to represent the whole neighbourhood radiation balance (URB_{tower})

and a second instrument was located 1.5 m above and in the centre of the rooftop (15 m long, >40 m wide considering contiguous rooftops) of the private property where the tower was installed to represent radiation balance over flat rooftops (URB_{roof}). URB_{roof} was located about 14 m E of URB_{tower} and any impact of shadowing was minor owing to the open nature of the tall tower and would have been restricted to late afternoon periods. Air temperature (T_{air}) was monitored at z_M with a PRT detector (models HMP45C-212 at URB and HMP45C at SUB and RUR, CSCC). A snow ranging sensor (model SR50, CSCC) measured snow depth (z_{snow}) over bare soil at RUR, in the backyard where the tower was installed at SUB, and on the rooftop of the private property where the tower was installed at URB. Supporting meteorological variables were averaged half-hourly before analysis.

At URB and SUB, an aluminium telescopic triangular lattice tower was used. The tower base was attached to the front of a 2.5 × 5 m closed trailer which was sitting in the backyard of a private property. The data logging equipment enclosed in the trailer and the base of the tower was accessible at the ground level. Eddy covariance instrumentation was mounted about 1 m upwind of the tower, relative to prevailing winds, on a boom which was installed about 1 m above the tower top section on a mast. At RUR, the eddy covariance instrumentation was mounted on a boom more than 1 m upwind, relative to prevailing winds, of the supporting tripod mast. The tripod itself was mounted beside and upwind of

an electric pole for logistical reasons. Hence, for all three sites flow distortion by the tower structure was minimized.

In accordance with our safety protocol, the flux towers at URB and SUB were retracted whenever high winds (>60 km/h), wind gusts (>70 km/h), or freezing precipitation were forecasted for the next 12–24 h. Hence, our measurements exclude those more extreme events likely associated with frontal passages.

2.3. Calculation of turbulent fluxes and quality control

Latent (Q_E) and sensible (Q_H) heat fluxes were calculated as the covariance of scalars (H_2O concentration and air temperature, respectively) and vertical wind velocity (Desjardins *et al.*, 1993; Baldocchi, 2003). Fluxes were calculated from block averages over 30-min time periods. Two rotations were applied to set mean lateral and vertical wind speed to zero (Tanner and Thurtell, 1969). A density correction was applied to Q_E as per Webb *et al.* (1980). No correction was applied for spectral loss or sensor separation as these corrections typically modify fluxes by only a few percent (Christen and Vogt, 2004). No provisions were made to account for the lack of energy balance closure as it cannot be reliably determined in urban environments.

Quality control procedures applied to meteorological variables as well as radiative and turbulent fluxes involved the exclusion of data points for time periods when absolute values of mean, minimum, maximum, or standard deviation were outside variable-specific realistic ranges. Data points from known periods of instrument malfunction, calibration, or servicing were also rejected. Q_E and Q_H were further quality controlled by discarding data points corresponding to half-hours when (1) less than two-third of raw data were usable to calculate fluxes; (2) the number of points identified as spikes was greater than 1% of the record length; (3) wind was blowing from behind the sonic anemometer–thermometer and through the tower structure; (4) the difference between block average and linear detrended fluxes was greater than the block average flux; or (5) dew, frost, rain, or snow obstructed the optical path of the gas analyzer as identified by monitoring the automatic gain control (AGC) value. Spikes in raw data records were identified as three or fewer consecutive points that were at least 3.5 standard deviations away from a running mean (2-min window) with an absolute value above a variable-specific threshold (Vickers and Mahrt, 1997). No filtering based on friction velocity (u^*) was applied. Meteorological and flux variables were visually inspected and remaining data points showing obvious unrealistic behaviour were excluded.

2.4. Data analysis

Measurements were performed continuously from fall 2007 to fall 2009. This study focuses on the two wintertime periods corresponding to measurements made from 1 December 2007 to 31 March 2008 and from 1 December 2008 to 31 March 2009. During the study

period, the towers were in the retracted position 28% of the time at both SUB and URB. For all three sites, only data when the towers at both URB and SUB were in the extended position were used. Hence for the study period, Q^* , Q_H , and Q_E were available 67, 38, and 38% of the time at RUR, 72, 52, and 52% at SUB, and 66, 39, and 38% at URB, respectively, after quality control and exclusion of retracted-tower periods.

The energy budget (terms in $W\ m^{-2}$) of the sites can be written as follows:

$$Q^* + Q_F = Q_H + Q_E + \Delta Q_S + \Delta Q_A + S \quad (1)$$

where Q_F is the anthropogenic heat flux, ΔQ_S the net change of heat storage, ΔQ_A the net-advedted flux, and S any other sources or sinks. ΔQ_A and S are assumed to be negligible because of the careful choice of sites and measurement heights and are thus neglected. When half-hourly Q^* , Q_E , and Q_H were all available, ΔQ_S was calculated as a residual term:

$$\Delta Q_S = (Q^* + Q_F) - (Q_E + Q_H) \quad (2)$$

Eddy covariance measurements typically suffer from the lack of energy balance closure that is about 20% over natural surfaces (Wilson *et al.*, 2002), therefore ΔQ_S is likely overestimated and represents an upper limit. It is worth noting that this residual term differs slightly from previously reported residual terms as we estimated Q_F which is usually not available in similar published studies.

Q_F was defined as

$$Q_F = Q_M + Q_V + Q_B \quad (3)$$

where Q_M is the heat loss from human metabolism, Q_V from vehicular traffic, and Q_B from the building sector. The methodology to estimate Q_F at SUB and URB is detailed in Appendix A1. Q_F was estimated from the period 2007–2009 although only Q_B varied for one year to the next, Q_M and Q_V were assumed constant between years. Q_F was also assumed to be negligible at RUR and was set at zero.

The stability parameter (ζ) was calculated as

$$\xi = \frac{(\zeta_M - \zeta_d)}{L} \quad (4)$$

where z_d is the zero-displacement height taken as 0.7 z_H at URB and SUB. At RUR, z_d was set equal to z_{snow} because flux measurements were made close to the surface and no canopy was present in wintertime. Obukhov length (L) was computed as per Monteith and Unsworth (1990).

A clearness index was calculated as follows:

$$k_T = \frac{K_{in}}{G_0} \quad (5)$$

where G_0 is the solar irradiance at the top of the atmosphere calculated as per Duffie and Beckman (2006) and

Table II. Monthly mean air temperature, total snowfall, and total precipitation measured at the Montreal Trudeau airport (Environment Canada, 2010).

	December	January	February	March
Year	2007	2008	2008	2008
Mean air temperature (°C)	-3.1	-2.0	-3.4	0.3
Total snowfall (cm)	112.8	56.6	88.0	77.8
Total precipitation (mm)	119.8	98.8	107.2	121.6
Year	2008	2009	2009	2009
Mean air temperature (°C)	-2.1	-8.9	-2.3	3.7
Total snowfall (cm)	97.0	71.7	34.8	2.6
Total precipitation (mm)	151.4	67.6	85.0	47.6
1971–2000 Normals				
Mean air temperature (°C)	-6.3	-10.2	-8.4	-2.3
Total snowfall (cm)	48.3	52.5	43.3	36.0
Total precipitation (mm)	81.3	78.3	61.5	73.6

Table III. Monthly daytime (night-time) means of environmental variables.

Year	Month	Site	T_{air} (°C)	K_{in} (W m ⁻²)	K_{out} (W m ⁻²)	L_{in} (W m ⁻²)	L_{out} (W m ⁻²)	Q^* (W m ⁻²)	α	z_{snow} (m)
2007	December	RUR	-8.4 (-9.9)	151	122	250 (248)	275 (266)	3 (-19)	0.82	0.26
		SUB	-7.9 (-8.8)	151	59	248 (245)	280 (272)	59 (-29)	0.42	0.31
		URB	-7.5 (-8.5)	142	64	246 (244)	284 (277)	39 (-35)	0.45	0.30
2008	January	RUR	-7.1 (-9.4)	204	146	238 (235)	280 (266)	16 (-32)	0.71	0.13
		SUB	-6.8 (-8.3)	209	66	230 (222)	282 (269)	91 (-49)	0.34	0.27
		URB	-6.5 (-7.7)	191	69	228 (223)	289 (276)	61 (-57)	0.36	0.07
	February	RUR	-5.9 (-7.1)	218	173	258 (265)	286 (278)	17 (-14)	0.81	0.25
		SUB	-6.2 (-7.0)	266	99	238 (246)	286 (278)	118 (-33)	0.40	0.54
		URB	-6.0 (-6.7)	240	101	239 (246)	292 (283)	85 (-39)	0.44	0.17
	March	RUR	-3.2 (-5.2)	367	276	250 (254)	296 (281)	45 (-29)	0.76	0.41
		SUB	-1.5 (-3.1)	332	114	256 (254)	308 (292)	166 (-40)	0.37	0.83
		URB	-2.1 (-3.1)	303	107	255 (254)	311 (295)	139 (-44)	0.39	0.19
	December	RUR	-8.6 (-9.0)	138	89	250 (251)	278 (273)	22 (-23)	0.64	0.17
		SUB	-8.2 (-8.1)	145	42	250 (251)	281 (277)	73 (-28)	0.32	0.20
		URB	-7.7 (-7.5)	130	41	243 (245)	286 (281)	45 (-38)	0.36	0.09
2009	January	RUR	-12.4 (-13.7)	209	175	223 (227)	258 (249)	0 (-23)	0.84	0.41
		SUB	-12.3 (-12.7)	211	77	218 (221)	260 (254)	91 (-35)	0.40	0.47
		URB	-11.9 (-11.8)	195	85	217 (221)	268 (262)	60 (-43)	0.44	0.17
	February	RUR	-6.8 (-8.7)	265	197	239 (240)	283 (270)	23 (-31)	0.75	0.36
		SUB	-6.2 (-6.9)	258	86	236 (239)	287 (277)	122 (-40)	0.36	0.50
		URB	-5.5 (-6.2)	229	69	239 (235)	298 (283)	101 (-51)	0.30	0.10
	March	RUR	-0.2 (-2.5)	355	96	249 (246)	316 (297)	193 (-53)	0.28	0.08
		SUB	0.3 (-1.7)	361	66	250 (246)	323 (299)	222 (-55)	0.20	0.39
		URB	2.2 (0.7)	320	42	261 (259)	346 (313)	192 (-57)	0.13	0.01

Daytime (night-time) corresponds to periods when $K_{\text{in}} \geq (<)5 \text{ W m}^{-2}$. Daytime α includes data between 10h00 and 14h00 LST. URB α corresponds to URB_{tower} α . z_{snow} was measured over bare soil at RUR, in a backyard at SUB, and on a rooftop at URB.

was used to quantify cloud cover and thus characterize light regime (diffuse vs direct light).

3. Results and discussion

3.1. Environmental conditions during the study period
The study period includes two winters with above-normal temperatures and very different precipitation regimes

(Table II). Winter 2007–2008 was generally colder than 2008–2009. Snowfall was above normal throughout winter 2007–2008 and the snow-cover period lasted from December to March (3 December 2007 to 8 April 2008 at RUR; Table III). In contrast in 2008–2009, snowfall was above normal only for the first half of the winter and liquid precipitation dominated during the second half, thus the snow-cover period was mostly restricted to

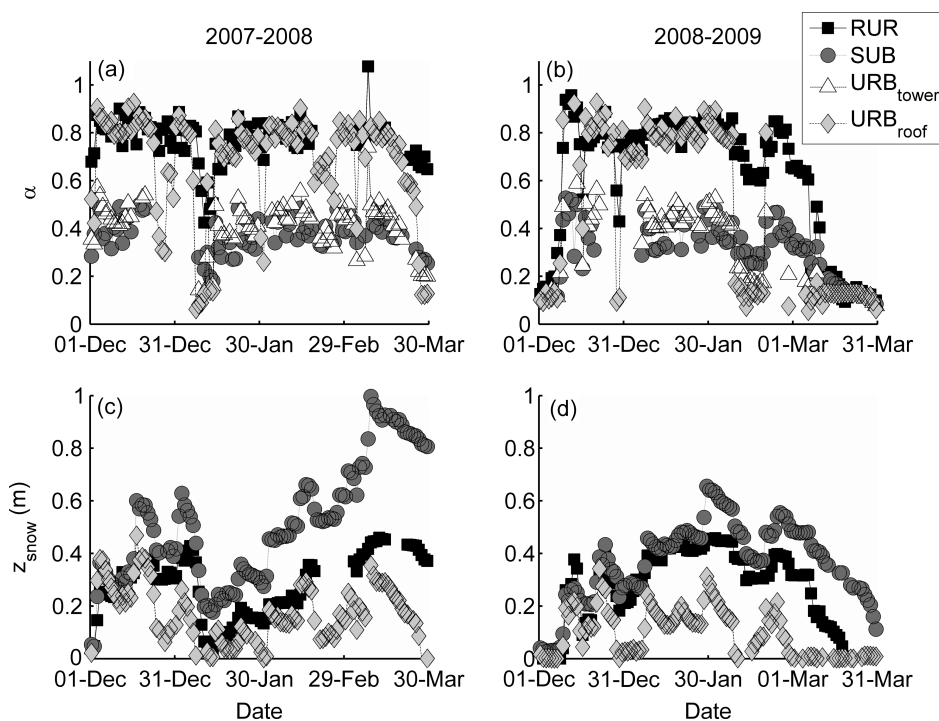


Figure 2. Daily average ($n > 3$) of (a, b) daytime (10h00 to 14h00 LST) albedo (α) and (c, d) whole day snow depth (z_{snow}). α was measured on a roof top (URB_{roof}) and at the top of the flux tower at URB (URB_{tower}). z_{snow} was measured over bare soil at RUR, in a backyard at SUB, and on a rooftop at URB.

January and February (10 December 2008 to 19 March 2009 at RUR; Table III).

3.2. Albedo

During the snow-cover period, α was twice as high at RUR (0.70–0.85) than SUB and URB_{tower} (0.30–0.45), while URB_{roof} α was similar to RUR (Table III, Figure 2(a) and (b)). In mid-February 2009 and also in early January 2008, URB_{tower} showed days with markedly decreased α (Figure 2(a) and (b)). This decrease was related to the absence of snow on rooftops (Figure 2(c) and (d)) and low URB_{roof} α (Figure 2(a) and (b)). Simple calculations based on the decrease in URB albedo at the tower and rooftop levels between snowy-roof and snow-free roof conditions suggest that rooftops accounted for 40% of the flux tower radiative footprint.

The effect of rooftop snow on the radiation balance was studied by comparing two 4-day periods with similar air temperature (mean diurnal variation between -5 and -10 °C) and wind regimes (SW–NW winds). The first period (snowy rooftops at URB) was 4–8 December 2007 with mean $z_{\text{snow}} = 0.35$ m on URB rooftop. The second period (snow-free rooftops at URB) was 13–17 February 2009 with mean $z_{\text{snow}} = 0.03$ m on URB rooftop. Note that rooftops were mostly snow covered at SUB during both periods.

Under snowy-roof conditions, mid-day α was lowest at SUB at 0.41 and slightly greater for URB_{tower} at 0.48, while α was 0.83 for URB_{roof}, similar to RUR at 0.82 (Figure 3(a)). Under snow-free roof conditions, α was lowest for URB_{roof}, with a mid-day value of 0.12 (Figure 3(b)). Consequently, the composite

URB_{tower} albedo was slightly lower than SUB, with mid-day values of 0.17 and 0.24, respectively (Figure 3(b)). Intra-urban variability in albedo during winter time can thus be significantly impacted by the presence of snow on rooftops, which in turn can differ with rooftop characteristics within urban areas as they did in this study (Table I). For example, most (>85%) buildings at URB were constructed before 1980, whereas about half of all the buildings were constructed after 1980 at SUB, suggesting that the thermal efficiency of rooftops is likely much lower at URB which could contribute to intra-urban snow cover and albedo variability.

SUB and URB_{tower} showed similar α values when rooftops were covered with snow but SUB was slightly lower than URB_{tower} overall (Table III) and was clearly lower on some days (Figure 2(a) and (b)). The difference between SUB and URB_{tower} albedo observed here was inconsistent with surface cover fractions, structure, and geometry of the sites (Table I). For example, SUB had greater vegetation cover fraction (mostly grass) that was basically snow covered, which would have promoted higher albedo. Also, URB had well defined street canyons and alley canyons (row buildings, greater aspect ratio z_H/W , Table I) that were expected to induce lower albedo than SUB (Kondo *et al.*, 2001; Fortuniak, 2008). However, the SUB : URB_{tower} α ratio was positively correlated with the clearness index k_T (Figure 4(a)). This result indicates that both sites had very similar α values under overcast conditions (diffuse light dominated), while URB_{tower} showed α up to 28% greater than SUB under clear sky conditions (direct light dominated). The SUB : URB_{tower} α ratio was also negatively correlated

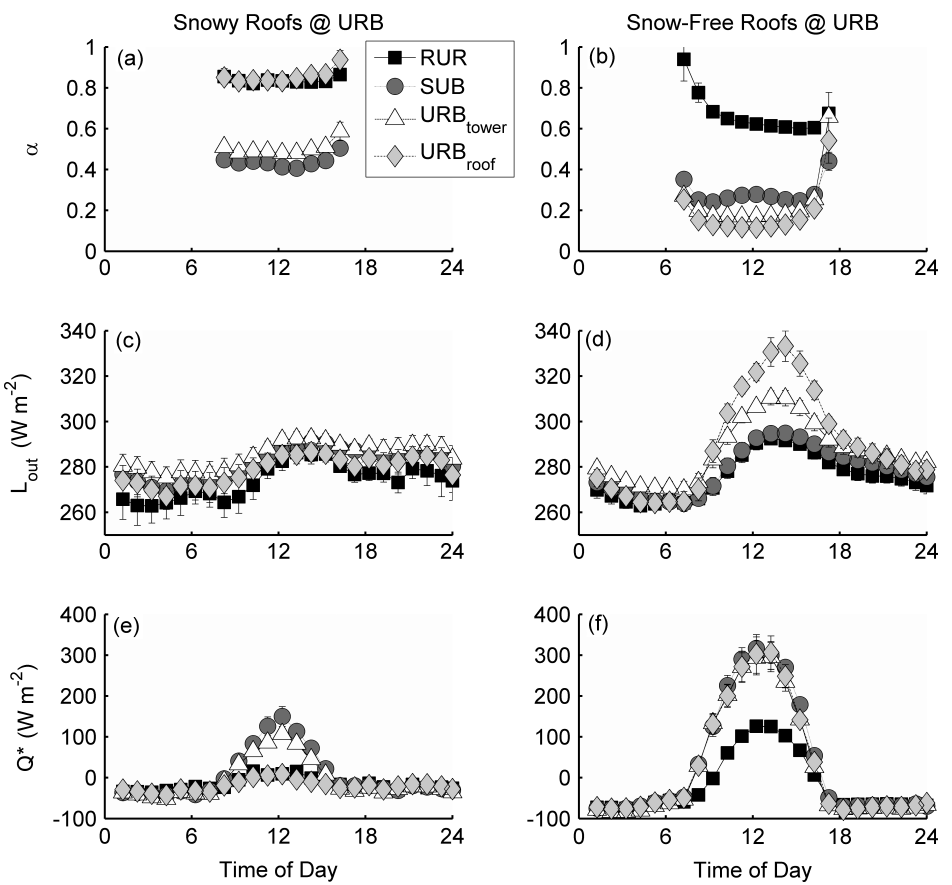


Figure 3. Diurnal ensemble average ($1 < n < 5$) of (a, b) daytime ($K_{in} > 5 \text{ W m}^{-2}$) albedo (α), (c, d) outgoing longwave radiation (L_{out}) and (e, f) net radiation (Q^*) for two 4-day wintertime periods when snow was and was not present on URB rooftops. See text for details.

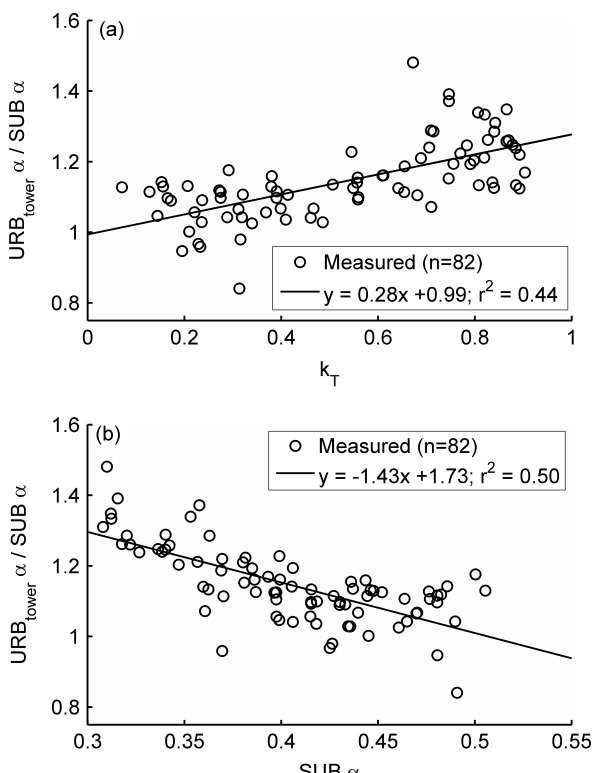


Figure 4. Daily ratio of URB over SUB daytime (10h00 to 14h00 LST) albedo (α) against (a) the daytime clearness index k_T and (b) SUB α for days when mean daily $z_{\text{snow}} > 0.1 \text{ m}$ and $\alpha > 0.3$ at URB. See text for details.

with SUB α (Figure 4(b)), while no significant relationship was found with URB_{tower} α , thus indicating that the between-site difference in albedo was because of the variability observed at SUB. At SUB, the buildings are detached and surrounded by relatively large snow-covered areas in winter. Under direct light, buildings shadow those snow-covered areas, inducing a decrease in the albedo of those surfaces which translates into a significant albedo decrease at the neighbourhood level. The same effect could have taken place around numerous tall coniferous trees and on the different facets of sloped roofs. This shadowing effect likely induces a milder albedo decrease in street and alleys canyons at URB because the underlying surfaces are darker and include a greater proportion of walls, which do not accumulate snow, and ploughed streets or alleys. Also, flat rooftops, generally bordered by edges of limited height, are not prone to shadowing effects.

3.3. Net radiation

In accordance with the between-site albedo differences observed during the snow-cover period, daytime Q^* was much higher at SUB and URB than RUR and was generally 20–30 W m^{-2} higher at SUB than URB over the course of the winter (Table III). The monthly mid-day (10h00 to 14h00 LST) difference in Q^* between SUB and URB was larger than the compensating greater

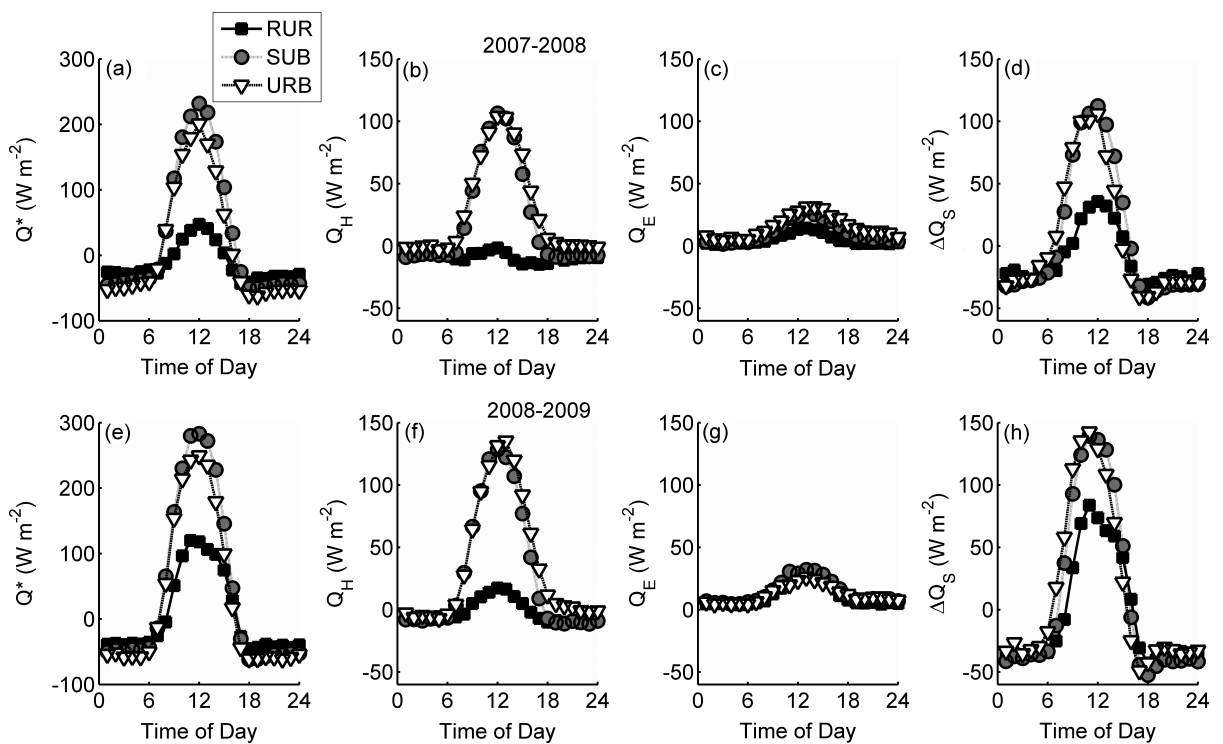


Figure 5. Diurnal ensemble average of energy balance components. Note the different scale used for Q^* . Hourly bins ($n > 30$) are shown for clarity.

Q_F at URB (Table V). Night-time Q^* was consistently 2–10 W m^{-2} higher at SUB than URB because of generally lower L_{out} at SUB (Table III). Q^* showed the smallest diurnal amplitude at RUR and highest amplitude at SUB while it was almost similar, yet slightly lower, at URB (Figure 5(a) and (e)). Q^* was higher at SUB than URB at all times except in the early morning when there was no difference between sites. The afternoon decline in Q^* began about 1 h earlier at URB than SUB. These results show that the albedo differences observed between urban areas induced significant intra-urban variability in net radiation during wintertime over Montreal, both seasonally and diurnally.

The presence of snow on rooftops influencing the sites' albedo significantly impacted the radiation budget of the studied urban areas. Under snowy-roof conditions, URB_{roof} showed no diurnal difference in Q^* as compared with RUR (Figure 3(e)). SUB and URB_{tower} showed markedly higher daytime Q^* than RUR with SUB being up to 50 W m^{-2} higher than URB_{tower} at noon (Figure 3(e)). Under snow-free roof conditions, SUB, URB_{tower}, and URB_{roof} showed daytime Q^* up to 200 W m^{-2} higher than RUR. The absence of snow on rooftops at URB induced significant daytime L_{out} increase from rooftop surfaces which increased daytime L_{out} at the neighbourhood level (Figure 3(d)). No such effect was observed at SUB where the roofs remained snow covered during both periods. Despite higher daytime L_{out} at URB_{tower} under snow-free roof conditions, mid-day Q^* was similar between URB_{tower} and SUB, suggesting that the decrease in α due to the absence of

Table IV. Mean wintertime daily totals ($\text{MJ m}^{-2} \text{ day}^{-1}$).

Sites	Q^*	Q_F	Q_H	Q_E	ΔQ_S
2007–2008					
RUR	-1.14	0.00	-0.74	0.45	-0.85
SUB	2.50	0.91	1.83	0.94	0.64
URB	1.12	3.14	2.46	1.33	0.47
2008–2009					
RUR	0.43	0.00	-0.15	0.97	-0.39
SUB	3.58	0.91	2.48	1.21	0.80
URB	2.34	2.97	3.13	1.07	1.11

For each site, only half-hours when all variables were available were used.

snow on rooftops at URB compensated for the lower α at SUB under snowy-roof conditions.

3.4. Anthropogenic heat flux

Total daily Q_F was about three times higher at URB than SUB (Table IV). Consequently, the total available energy ($Q^* + Q_F$) was highest at URB despite higher Q^* being observed at SUB on a full daily cycle. Also, total daily Q_F was of the same magnitude as Q_H at URB and accounted for up to half of Q_H at SUB (Table IV). Daytime $Q^*/(Q^* + Q_F)$ ranged from 0.91 to 0.98 and from 0.71 to 0.93 at SUB and URB, respectively (Table V). These results show that Q_F is a significant term of the energy balance over Montreal residential areas in winter, especially in December when K_{in} and Q^* are lowest, and can account for up to 9–29% of daytime total available energy.

Table V. Daytime (10h00 to 14h00 LST) monthly means of Q^* and Q_F and ratios of Q^* , Q_H , Q_E , and ΔQ_S over $(Q^* + Q_F)$.

Year	Month	Site	Q^* (W m ⁻²)	Q_F (W m ⁻²)	$Q^*/(Q^* + Q_F)$	$Q_H/(Q^* + Q_F)$	$Q_E/(Q^* + Q_F)$	$\Delta Q_S/(Q^* + Q_F)$
2007	December	RUR	12	0	1.00	-0.83	1.00	0.83
		SUB	113	11	0.91	0.44	0.13	0.43
		URB	92	37	0.71	0.49	0.19	0.32
2008	January	RUR	48	0	1.00	-0.06	0.27	0.79
		SUB	178	11	0.94	0.46	0.11	0.43
		URB	130	38	0.77	0.49	0.13	0.38
	February	RUR	39	0	1.00	-0.05	0.25	0.80
		SUB	229	11	0.95	0.47	0.09	0.44
		URB	192	38	0.83	0.48	0.11	0.41
	March	RUR	63	0	1.00	-0.03	0.27	0.76
		SUB	338	10	0.97	0.40	0.11	0.49
		URB	282	36	0.89	0.39	0.13	0.48
	December	RUR	63	0	1.00	0.33	0.34	0.33
		SUB	141	11	0.93	0.54	0.13	0.33
		URB	111	35	0.76	0.50	0.14	0.36
2009	January	RUR	12	0	1.00	0.00	0.50	0.50
		SUB	182	12	0.94	0.45	0.07	0.48
		URB	128	40	0.76	0.45	0.10	0.45
	February	RUR	66	0	1.00	0.26	0.30	0.44
		SUB	271	11	0.96	0.46	0.10	0.44
		URB	243	36	0.87	0.43	0.08	0.49
	March	RUR	301	0	1.00	0.10	0.18	0.72
		SUB	420	9	0.98	0.38	0.12	0.50
		URB	375	30	0.93	0.48	0.07	0.45

For each site, only half-hours when all variables were available were used.

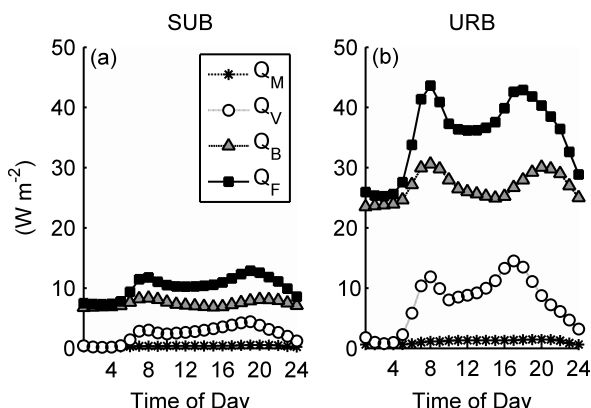


Figure 6. Diurnal ensemble average of wintertime (1 December 2007 to 31 March 2008) anthropogenic heat flux components at the (a) suburban and (b) urban sites (see Appendix A1 for details).

Figure 6 shows Q_F and its components for SUB and URB as determined for the period 1 December 2007 to 31 March 2008. Q_F ranged from 7 to 13 W m^{-2} and from 25 to 45 W m^{-2} at SUB and URB, respectively. Peak hours were around 7h00–8h00 and 18h00–19h00 LST at both sites when Q_V reached its maximum. Q_B dominated Q_F , while Q_M was negligible at both sites. Our Q_F estimates for residential areas in Montreal are lower than those reported by Summers (1965 in Klyskik, 1996), Oke (1997), and Taha (1997). However, these latter estimates included

denser parts of the city (downtown business district) and areas enclosing industrial activities, which were excluded from our estimates. Also, Q_B was estimated using energy consumption data from warm winters (Table II), inducing lower estimations of Q_B and Q_F relative to normal or below-normal years. Nevertheless, the diurnal trends described here are consistent with other studies (Ichinose *et al.*, 1999; Sailor and Lu, 2004; Offerle *et al.*, 2005, Pigeon *et al.*, 2007).

Q_F between-year variability was only due to Q_B through (1) year-specific annual energy consumption totals and (2) temperature regimes which determined the distribution of space heating annual totals within each year. As a consequence, the Q_F between-year variability was negligible at SUB and rather small at URB (Table IV) and hourly estimates for the period 1 December 2008 to 31 March 2009 were within 1 W m^{-2} of those in Figure 6.

These estimates represent a first attempt to quantify the diurnal and seasonal variability of Q_F over Montreal. However, their uncertainty is unknown and sources of bias are expected. The greatest source of error is likely the population density estimates which were taken at the borough level to match the available information on population displacements. These estimates are expected to be lower than the population density at the neighbourhood level (e.g. 1 km radius around the flux tower) as

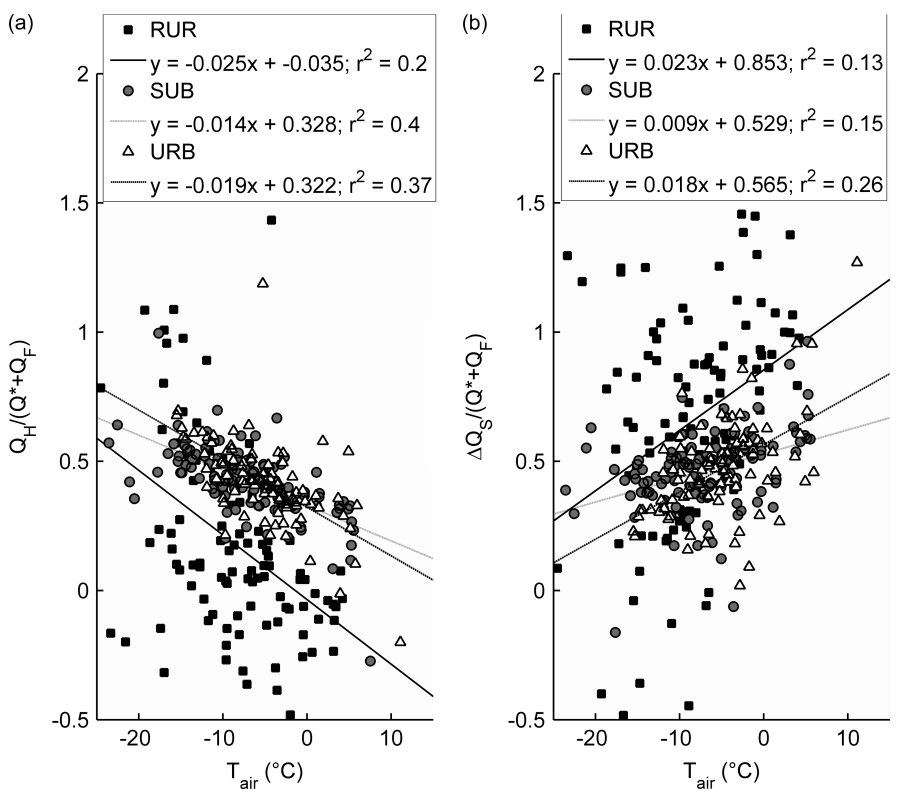


Figure 7. Ratios of (a) mean daytime (10h00 to 14h00 LST) Q_H and (b) ΔQ_s over $(Q^* + Q_F)$ as a function of air temperature (T_{air}).

this latter scale does not include mid- to large-sized parks. Hence, Q_F estimates may suffer from an underestimation. Also, because population density was fixed, any seasonality is not represented; this source of uncertainty is expected to have more of an impact on summer Q_V . In calculating Q_B , residential households and commercial/institutional floorspace comprising the study sites were assumed to be similar to the province-wide average. As the province-wide average is biased towards Montreal as this region represents about half the provincial population, this source of uncertainty is likely minor. Despite these minor limitations, the Q_F estimates reported here represent the most detailed information on heat loss from human activity available to date for Montreal.

3.5. Sensible heat flux

Total daily Q_H was higher at URB than SUB in both years (Table IV), which is in accordance with surface cover fractions (Table I). Total daily Q_H was higher in 2008–2009 than in 2007–2008 at all sites, which is consistent with total Q^* . Overall, monthly means of daytime $Q_H/(Q^* + Q_F)$ tended to decrease from about 0.5 to about 0.4 throughout the winter at both SUB and URB (Table V). Daytime $Q_H/(Q^* + Q_F)$ was generally higher at URB than SUB, especially in March 2009 when snow cover disappeared earlier at URB (Table III).

At the daily time scale, daytime ratios of $Q_H/(Q^* + Q_F)$ were negatively correlated with T_{air} which explained 20, 40, and 37% of $Q_H/(Q^* + Q_F)$ variability at RUR, SUB, and URB, respectively (Figure 7(a)). At RUR, $Q_H/(Q^* + Q_F)$ had the same sign as T_{air} and was around

0 when $T_{air} = 0^{\circ}C$. This was expected as the sign of Q_H in winter over a crop field covered with snow depends on the temperature gradient between the air and the snowpack, the latter being around $0^{\circ}C$. $Q_H/(Q^* + Q_F)$ was consistently lower at RUR than SUB and URB at any temperature. A coincidental regression test (Zar, 1984) indicated that regressions of $Q_H/(Q^* + Q_F)$ with T_{air} were not significantly different between SUB and URB [$F = 2.69$, degrees of freedom = (2; 218)]. It is worth noting that the equilibrium temperature of $Q_H/(Q^* + Q_F)$ [temperature at which $Q_H/(Q^* + Q_F)$ would change sign] lies between 16 and 24°C, which corresponds to typical indoor temperatures in Montreal. This result suggests that the indoor–outdoor temperature gradient might help explain the temporal variability of daily daytime $Q_H/(Q^* + Q_F)$ during the winter time over temperate cities through the regulation of heat conduction from indoor to outdoor air. Assuming that the variability in outdoor air temperature is compensated for by building heating (Q_B) to keep indoor temperature, and thus the amount of energy stored in the indoor air volume, constant, an increase in the indoor–outdoor temperature gradient would increase heat conduction from indoor to outdoor and thus increase Q_H . However, a more detailed study on the interaction of these energy balance terms would be needed to shed light on this phenomenon.

Q_H showed a marked diurnal trend that demonstrated the departure of SUB and URB from RUR (Figure 5(b) and (f)). Similar wintertime trends have been reported for other temperate cities highlighting the effect of urbanization on sensible heat loss (Grimmond, 1992;

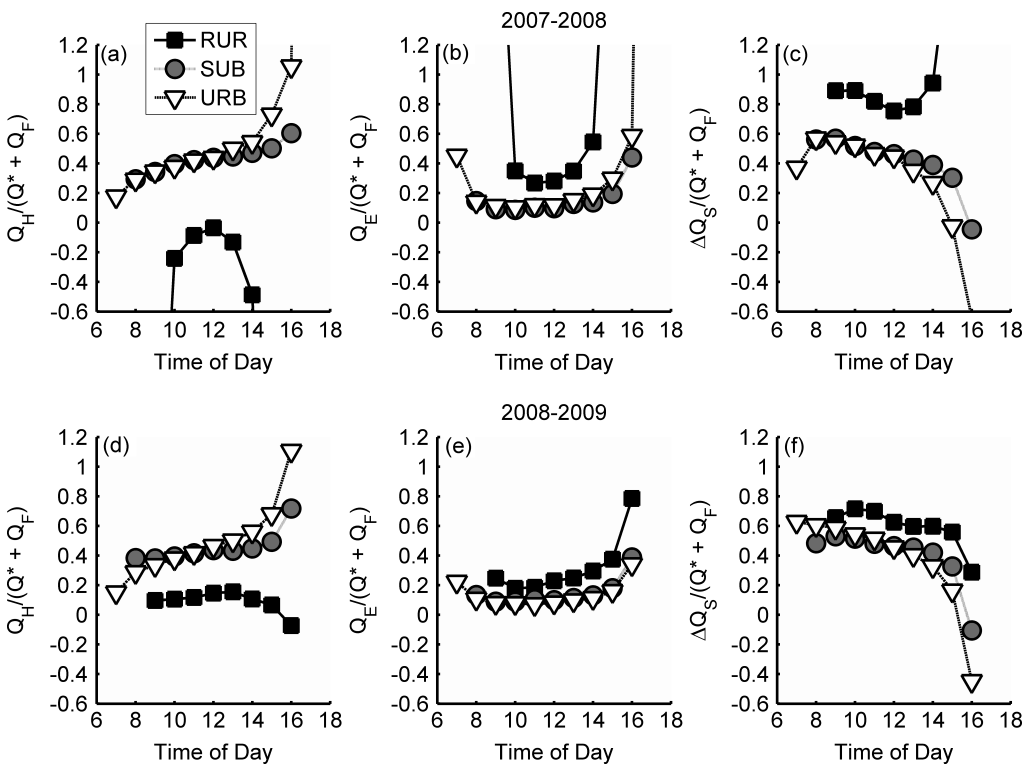


Figure 8. Ratios of (a, d) Q_H , (b, e) Q_E , and (c, f) ΔQ_S over $(Q^* + Q_F)$ for periods when $(Q^* + Q_F) > 0 \text{ W m}^{-2}$. Hourly bins ($n > 30$) are shown for clarity.

Offerle *et al.*, 2006; Vesala *et al.*, 2008). Although similar trends were observed, Q_H peaked about 1 h later at URB than SUB (Figure 5). Consequently, URB showed greater $Q_H/(Q^* + Q_F)$ than SUB after noon (Figure 8(a) and (d)). Daytime $Q_H/(Q^* + Q_F)$ increased throughout the day at both sites with a greater increase in the afternoon. In the early morning, no marked between-site difference in Q_H was apparent but URB showed lower $Q_H/(Q^* + Q_F)$ than SUB which was mostly because of higher Q_F (Figure 6).

Q_H decreased to a slightly positive and negative value in the evening at URB and SUB, respectively (Figure 5(b) and (f)). Christen and Vogt (2004) reported a similar night-time difference between the urban and suburban sites for a summertime period and related this difference to more frequent non-stable conditions of the near-surface air layers at the denser sites. Similarly, URB showed less frequent stable conditions than SUB during the study period (Figure 9), hence, the stability regime could also affect intra-urban differences in night-time Q_H over Montreal during winter time.

3.6. Latent heat flux

Total daily Q_E was on average higher in 2008–2009 at both RUR and SUB, corresponding to the winter with most amount of liquid water readily available for evaporation from rainfall (Table I) and snowmelt (Table III, Figure 2) and sublimation from snow. In contrast at URB, total daily Q_E was higher in 2007–2008 than in 2008–2009 when the long snow-cover period promoted evaporation through a constant supply of snow to melt

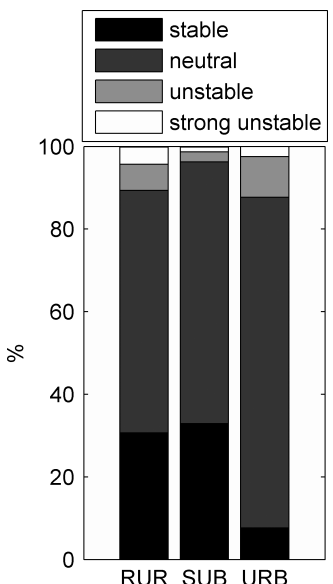


Figure 9. Histogram of near-surface stability. Stable conditions correspond to $10 > \zeta > 0.1$, neutral to $0.1 > \zeta > -0.1$, unstable to $-0.1 > \zeta > -0.5$, and strong unstable to $-0.5 > \zeta > -100$. $n = 1313$ co-incident half-hours.

from rooftops and streets. Hence, Montreal showed intra-urban differences in terms of the water vapour emission response to wintertime climatic conditions.

Total daily Q_E averaged over both winters was 0.71, 1.08, and $1.20 \text{ MJ m}^{-2} \text{ day}^{-1}$ at RUR, SUB, and URB, respectively (Table IV), which is slightly lower than the wintertime values reported by Christen and Vogt (2004)

for a denser temperate European city. The daily Q_E totals reported from our sites are also much lower than those measured over a site exposed to much milder winter conditions with frequent rainfall in Vancouver, Canada (Grimmond, 1992). Our results show that water vapour emissions in wintertime were 51–69% higher over urban areas relative to the rural baseline. The main sources of water vapour include combustion from vehicular traffic and heating fuels as well as snow sublimation/evaporation from different surfaces, especially rooftops and roads. The increase in water vapour emissions with urbanization is consistent with the between-site differences in the distribution of those sources as indicated by Q_V , Q_B (Figure 6), λ_P , and λ_I (Table I).

The monthly mean daytime $Q_E/(Q^* + Q_F)$ was generally constant around 0.1 at both SUB and URB (Table V). Also, Q_E showed minimal diurnal variation at all three sites (Figure 5(c) and (g)) and $Q_E/(Q^* + Q_F)$ was very similar between SUB and URB throughout daytime hours at values below 0.2 (Figure 8(b) and (e)). A significant relationship between daily daytime $Q_E/(Q^* + Q_F)$ and any environmental variable could not be found at any site (data not shown). However, most high $Q_E/(Q^* + Q_F)$ values (>0.2) were associated with values of the stability index (ζ) between -0.1 and 0.1 , i.e. neutral conditions (Figure 10). Hence, high $Q_E/(Q^* + Q_F)$ values appeared to be restricted to specific meteorological events occurring in neutral stability conditions, suggesting that $Q_E/(Q^* + Q_F)$ is basically constant within and between days over snow covered, urbanized sites in winter, at least under unstable conditions.

3.7. Net change of heat storage

Mean total daily ΔQ_S was positive at both SUB and URB on a wintertime basis (December–March; Table IV) although mean total daily ΔQ_S was negative from October to January and positive the rest of the time (not shown). Other studies reported negative net change of heat storage during wintertime (Christen and Vogt, 2004; Offerle *et al.*, 2005; Offerle *et al.*, 2006) but

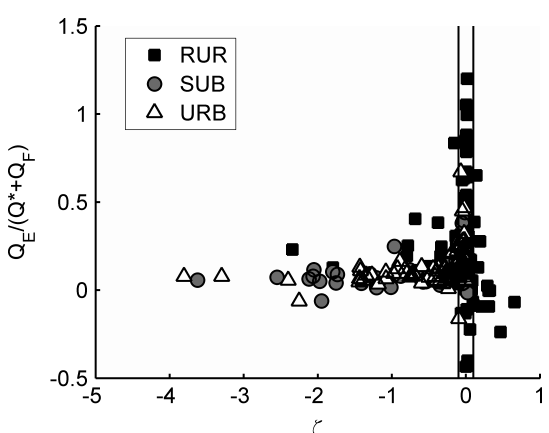


Figure 10. Ratio of mean daytime (10h00 to 14h00 LST) Q_E over $(Q^* + Q_F)$ as a function of the stability parameter ζ . Vertical bars enclose neutral conditions ($0.1 > \zeta > -0.1$).

these studies did not calculate Q_F separately from the residual term ΔQ_S . Between-year variability of ΔQ_S was consistent with that of Q^* , while between-site variability for the winter as a whole was mostly due to that of Q_E (Table IV). These results suggest that intra-urban differences in ΔQ_S during the winter depend on net radiation and (lack of) liquid water available to evaporate (see previous section).

Overall, the monthly mean daytime $\Delta Q_S/(Q^* + Q_F)$ generally increased from about 0.35 to about 0.45–0.5 (Table V). Daily daytime $\Delta Q_S/(Q^* + Q_F)$ was positively correlated with T_{air} at all sites and T_{air} explained 13, 15, and 26% of $\Delta Q_S/(Q^* + Q_F)$ variability (Figure 7(b)). $\Delta Q_S/(Q^* + Q_F)$ was consistently higher at RUR than SUB and URB for any given temperature which is in accordance with the correlation found between $Q_H/(Q^* + Q_F)$ and T_{air} . A coincidental regression test (Zar, 1984) indicated that regressions of $\Delta Q_S/(Q^* + Q_F)$ with T_{air} were not significantly different between SUB and URB [$F = 0.05$, degrees of freedom = (2; 215)]. Hence, the temporal variability of the net change of heat storage was correlated to air temperature with no sensitivity with respect to intra-urban difference in surface characteristics.

ΔQ_S diurnal variability was of similar amplitude at URB and SUB although buildings are generally smaller and sparser at SUB (Figure 5(d) and (h)). However, snow is removed from streets and rapidly melts from flat roofs at URB while it accumulates as relatively undisturbed snowpacks in front and back yards and in dense and high snowbanks along most streets at SUB. Hence, the different snow accumulation regimes can likely compensate to some extent for the lower building density in terms of heat storage. The similar ΔQ_S diurnal amplitude at both SUB and URB also suggests that the net change in heat storage in urban environments is independent from the total amount of heat stored as expected from building density, assuming that ΔQ_S estimates do not suffer from site-specific systematic errors (e.g. lack of energy balance closure).

URB and SUB showed the highest and lowest ΔQ_S values at mid-day and late afternoon, respectively (Figure 5(d) and (h)). Similar diurnal trends have been reported for different urban densities and climatic conditions (Grimmond, 1992; Christen and Vogt, 2004; Spronken-Smith *et al.*, 2006; Coutts *et al.*, 2007). However, the ΔQ_S morning increase and afternoon decrease occurred about 1 h earlier at URB than SUB (Figure 5(d) and (h)), while $\Delta Q_S/(Q^* + Q_F)$ was similar between SUB and URB before noon (Figure 8(c) and (f)). Except for early morning hours when $(Q^* + Q_F) > 0 \text{ W m}^{-2}$ and $Q^* < 0 \text{ W m}^{-2}$ at URB, $\Delta Q_S/(Q^* + Q_F)$ reached a maximum of about 0.6 around 8h00 LST at both sites and decreased thereafter. After noon, $\Delta Q_S/(Q^* + Q_F)$ dropped earlier and faster at URB than SUB which is consistent with between-site difference in Q^* (Figure 5(a) and (e)). URB showed higher early morning ΔQ_S than SUB induced by greater Q_F (Figure 6). These results indicate that intra-urban differences in the diurnal course

of ΔQ_S , especially in the afternoon, are to be expected over temperate, snow-covered cities during winter time.

Measurements of Q_H and Q_E with the eddy covariance technique have been showed to suffer from systematic underestimation due to the lack of energy balance closure (Wilson *et al.*, 2002) which appears to be because of the theoretical or methodological rather than instrumental issues (Foken, 2008). Hence, estimates of ΔQ_S calculated as a residual term should be considered as an upper limit. It is also worth noting that the energy used for water phase changes between liquid water, snow, and ice, which can be significant during snowmelt (Leroyer *et al.*, 2010), and water draining in the sewer system was not included in our Q_E measurements and might have affected our ΔQ_S estimates. However, this study showed that independent estimates of Q_F , which is a significant term of the energy budget of high latitude cities during wintertime, can be used to estimate ΔQ_S at fine time scale.

4. Conclusions

This study reports on the radiation and energy balances of three sites located along an urbanization gradient in the Montreal region for two wintertime (December–March) periods in 2007–2009. This study represents a first opportunity to analyse a unique two-year data set from a city with cold and snowy winters that will be used to validate and refine urban climate process models, especially regarding snow.

During the snow-cover period, the urban and suburban sites showed similar albedo (~ 0.4) which was about half that at the rural site (~ 0.8). The seasonal variability of the urban site's albedo was primarily affected by the presence of snow on rooftops; snow here tended to melt rapidly and rooftops represented about 40% of the radiative footprint area. The decrease in albedo due to the absence of snow on rooftops at the urban site induced greater net radiation (Q^*) overall despite increased daytime longwave radiation losses at the neighbourhood level. The suburban site showed lower albedo by up to 0.05 as compared to the urban site, which resulted in generally higher daytime net radiation. The albedo ratio of the two urbanized sites varied with a sky clearness index. The geometry of the suburban site, including the distribution of tall trees, along with relatively extended snow-covered areas between buildings and trees likely induced a site-specific response in albedo to cloudiness resulting in greater variability in albedo with direct-beam radiation at the suburban site.

This study presents the first estimates of hourly anthropogenic heat flux (Q_F) over residential areas in Montreal. Q_F was $7\text{--}13 \text{ W m}^{-2}$ at the suburban site and $25\text{--}45 \text{ W m}^{-2}$ at the urban site. Q_F was dominated by heat loss from buildings, while vehicular traffic contributed to rush hour peaks at both sites. Mean daily Q_F was of the same magnitude as sensible heat flux (Q_H) at the urban site and up to half of Q_H at the suburban site, while daytime Q_F accounted for up to

9–29% of the total available energy ($Q^* + Q_F$). Higher Q_F compensated for lower Q^* at the urban site which showed higher ($Q^* + Q_F$) overall on a daily basis. Thus Q_F represented a significant term of the energy budget over Montreal urban areas during wintertime.

The total available energy was mostly dissipated as sensible heat flux at the beginning of the winter season and was mostly stored towards the end of the winter at both urbanized sites. Both $Q_H/(Q^* + Q_F)$ and $\Delta Q_S/(Q^* + Q_F)$ showed significant correlation with air temperature at all three sites and regressions were not significantly different between the urban and suburban sites. The correlations of daytime $Q_H/(Q^* + Q_F)$ and $\Delta Q_S/(Q^* + Q_F)$ with T_{air} indicate that as air temperature decreases in wintertime, available energy is released as sensible heat flux more than it is stored, independently from any intra-urban variability in neighbourhood characteristics.

Water vapour emissions over Montreal in wintertime were low and accounted for a small fraction (10%) of total available energy during daytime at the urbanized sites. However, water vapour emissions were 51–69% greater at the urbanized sites than the rural baseline, which was consistent with between-site differences in expected emission sources. Water vapour fluxes show intra-urban variability in their response to between-year differences in climatic conditions.

Urbanized sites showed a distinct diurnal variability in energy balance components, except for Q_E . Mid-day Q^* and Q_H were 2–5 times and about an order of magnitude greater at the urbanized sites than the rural site, respectively. ΔQ_S was maximal in early morning and minimal in late afternoon and showed similar diurnal amplitude at both urbanized sites. These results suggest that the net change of heat storage in urban environments is independent from the total energy stored that would be expected from building structure and density. The total available energy was mostly stored before noon and dissipated as Q_H in the afternoon at both urbanized sites. However, the urban site showed earlier and more rapid changes in energy partitioning between Q_H and ΔQ_S than the suburban site. The atmospheric stability regime induced intra-urban differences in night-time Q_H over Montreal during winter time.

These observations, along with the underlying data set, can be used to refine, validate, and calibrate urban climate models in terms of the influence of snow, anthropogenic heat flux, and the intra-urban variability in structure and composition of urban features, on the radiation and energy balance of a Canadian temperate city during winter time.

Acknowledgements

This study was funded through a grant to Drs J. Voogt and T. R. Oke and IBS by the Canadian Foundation for Climate and Atmospheric Sciences (CFCAS). Post-doctoral funding to OB was provided by CFCAS. The authors wish to thank the assistance of Mitchell Lavoie

for the Q_F estimates, Olivier Gagnon (Environment Canada) for vehicular traffic profiles, and Jinfei Wang (University of Western Ontario) for the surface cover classification. The field and technical assistance of Eric Christensen, Kenton Ollivierre, Pierre-Luc Lizotte, Josée Thibodeau, Jean-François Aublet at McGill, and Dr Frédéric Chagnon and Bruno Harvey at Environment Canada is greatly appreciated.

A1. Appendix

A1.1. Estimating anthropogenic heat flux

Hourly anthropogenic heat flux (Q_F) was estimated using an approach based on Sailor and Lu (2004) and adapted to the available data for the urban and suburban sites. The general approach was to estimate each term separately (human metabolism, vehicular traffic, and building sector) by calculating hourly per reference unit (person, vehicle, household, or floor space m^2) heat release and multiplying by hourly number of units per surface area (population, vehicle, household, or floor space m^2 density) for the corresponding site. The reference unit used here differed somewhat from that of Sailor and Lu (2004), who strictly used a per capita approach, given the available data for the Montreal region. Daylight savings time was accounted for when appropriate.

A1.2. Hourly population densities

Hourly population densities (ρ_{pop}) were estimated separately for weekdays and weekends. Night-time (18h00 to 6h00 on weekdays, 18h00 to 9h00 on weekends) ρ_{pop} was calculated as the total number of inhabitant in the borough from 2006 census data over total borough surface area (Ville de Montréal, 2009a). At SUB, three large parks (201, 288, and 159 ha; Ville de Montréal, 2009b) were removed from borough surface area as these are considered as natural reserves more than urban parks. Daytime ρ_{pop} was calculated using borough's total population after accounting for work, school, shopping, and/or leisure displacements into, out of, and within each borough according to the Agence métropolitaine de transport's Fall 2003 origin-destination survey (AMT, 2009a). All displacements were considered for weekdays and only shopping and leisure displacements for weekends. As per Sailor and Lu (2004), transition periods (7h00 and 17h00 on weekdays and 10h00 and 17h00 on weekends) were linearly interpolated.

A1.3. Heat from human metabolism (Q_M)

Q_M was defined as follows:

$$Q_M = pcHM \cdot \rho_{\text{pop}} \quad (\text{A1})$$

where $pcHM$ is the per capita rate of heat from human metabolism (W person^{-1}) and ρ_{pop} is hourly population density (person m^{-2}). $pcHM$ was set to 175 and 75 W

person^{-1} during daytime and night-time, respectively (Sailor and Lu, 2004). Q_M was linearly interpolated during transition periods (6h00 and 22h00 on weekdays and 9h00 and 22h00 on weekends based on Q_V profiles).

A1.4. Heat from vehicular traffic (Q_V)

Hourly Q_V was calculated as follows:

$$Q_V = pvDVD \cdot N_V \cdot F_t \cdot \rho_{\text{pop}} \cdot EV \quad (\text{A2})$$

where $pvDVD$ is the per vehicle daily vehicle distance ($\text{km vehicle}^{-1} \text{day}^{-1}$), N_V the number of vehicle per person ($\text{vehicles person}^{-1}$), F_t the fraction of daily traffic per hour (day hour^{-1}), and EV the amount of energy released per vehicle per distance travelled (J km^{-1}). $pvDVD$ was calculated as the total vehicle kilometres travelled (aggregating vehicle types) for all $1 \times 1 \text{ km}$ cells comprising road segments with traffic count estimates around the flux towers, divided by traffic counts for one segment along each road with data according to the Agence métropolitaine de transport's 1998 origin-destination survey (AMT, 2009b). N_V was taken from 2003 origin-destination survey (AMT, 2009a). For weekdays, all vehicle classes (car, light truck, and heavy truck) were included, while heavy trucks were excluded for weekend estimates. Weekday F_t was computed using simulated displacements along a simplified road network within an approximately 3 km radius of each site for a weekday in January 2009 (Olivier Gagnon, personal communication) based on vehicle counts by class from the 2003 origin-destination survey (AMT, 2009a)). Weekend F_t was taken from Noriega *et al.* (2006). EV was calculated as follows:

$$EV = \frac{NHC \cdot \rho_{\text{fuel}}}{FE} \quad (\text{A3})$$

where NHC is the net heat of combustion of gasoline ($45 \times 10^6 \text{ J kg}^{-1}$), ρ_{fuel} the optimal fuel density of gasoline (0.75 kg l^{-1}), and FE the fuel economy (l km^{-1}). NHC and ρ_{fuel} were taken from Sailor and Lu (2004). FE was taken as a weighted average over vehicle MOBILE 6 classes (EPA, 2009) for each study site.

A1.5. Heat from the building sector (Q_B)

Q_B was estimated from energy consumption information assuming all the energy consumed was ultimately lost as heat. Annual energy consumption data by province were available publicly for the period 1990–2007 from the Natural Resource Canada's Office of Energy Efficiency (OEE, 2010). These data included energy efficiency (consumption per unit of space) stratified by sector, energy sources, end-use, and house or activity type but lacked information on intra-annual variability. In temperate regions, climate and people's behavior determine the temporal variability of energy demand for space heating and appliance use (Sailor *et al.*, 1998; Yao and

Steemers, 2005; Hamilton *et al.*, 2009). Thus Q_B was divided into two end-uses:

$$Q_B = Q_{Bh} + Q_{Ba} \quad (\text{A4})$$

where Q_{Bh} is the heat lost from space heating and Q_{Ba} the appliance use or non-space heating. Q_{Bh} is temperature-dependant and includes all energy sources except the fraction of electricity consumption that corresponds to Q_{Ba} which is temperature-independent. To estimate Q_B around our sites, only the residential and commercial/institutional sectors were relevant. House types within the residential sector were treated separately, while no distinction was made between activity types for the commercial/institutional sector. Energy efficiency was expressed on a per household basis and on a per floorspace m^2 basis for the residential and commercial/institutional sectors, respectively.

Annual energy efficiency for the period 2000–2007 was extrapolated to 2008 and 2009 using a relationship with mean wintertime (January–March and December) air temperature at the Montreal Trudeau airport (Environment Canada, 2010) and with time for space heating and non-space heating, respectively. Annual Q_{Bh} and Q_{Ba} were calculated by multiplying energy efficiency by number of household (residential) or by floorspace m^2 (commercial/institutional) per ground surface area estimated from a GIS database along 14 census tracks and 13 dissemination areas within a radius of about 1 km around the urban and suburban sites, respectively. Commercial/institutional floor space m^2 was estimated as building dimensions estimated from a GIS database multiplied by number of floors assessed visually from aerial photographs (Bing Maps, 2009).

Annual Q_{Bh} and Q_{Ba} were divided into hourly profiles following different methodologies. For Q_{Bh} , hourly air temperature data measured at the Montreal Trudeau airport for the period 2007–2009 (Environment Canada, 2010) was used to calculate a heating degree-hour index (HDHi) using a reference temperature of 18°C following Sailor and Vasireddy's (2006) work. Fractional HDHi was obtained on an annual basis by dividing hourly HDHi by the sum of all HDHi for each year and was then multiplied by annual Q_{Bh} to get hourly Q_{Bh} . For Q_{Ba} , energy consumption was assumed constant for one day to the next within each year and daily Q_{Ba} was obtained by dividing annual Q_{Ba} by the number of days of each year. Separate diurnal fractional profiles for domestic and non-domestic uses were taken from Hamilton *et al.* (2009) and were multiplied by daily Q_{Ba} to get hourly Q_{Ba} .

References

- AMT. 2009a. Résultats enquête O-D 2003. Centre d'information métropolitain sur le transport urbain. Agence Métropolitaine de transport. Accessed in July 2009.
- AMT. 2009b. Tableaux par secteur municipal enquête O-D 1998. Centre d'information métropolitain sur le transport urbain. Agence Métropolitaine de transport. [accessed July 2009] <<http://www.cimtu.qc.ca/EnqOD/1998/Resultats/Mobilite/Tableaux-sec.asp>>
- Baldocchi DD. 2003. Assessing the eddy covariance technique for evaluating carbon dioxide exchange rates of ecosystems: past, present and future. *Global Change Biology* **9**(4): 479–492.
- Bing Maps. 2009. Bing Maps, Bing Beta. Microsoft. Accessed in August 2009. <<http://www.bing.com/maps/>>
- Christen A, Vogt R. 2004. Energy and radiation balance of a central European city. *International Journal of Climatology* **24**(11): 1395–1421.
- Coutts AM, Beringer J, Tapper NJ. 2007. Impact of increasing urban density on local climate: spatial and temporal variations in the surface energy balance in Melbourne, Australia. *Journal of Applied Meteorology and Climatology* **46**(4): 477–493.
- Desjardins R, Rochette P, Pattey E, MacPherson I. 1993. Measurements of greenhouse gas fluxes using aircraft- and tower-based techniques. Agricultural effects on trace gases and global climate change. vol. ASA special publication 55. 45–62.
- Duffie JA, Beckman WA. 2006. *Solar Engineering of Thermal Processes*, John Wiley and Sons Inc.: Hoboken, NJ.
- Environment Canada. 2010. *Climate Data Online, National Climate Data and Information Archive*. Environment Canada. Accessed in March 2010. <http://www.climate.weatheroffice.ec.gc.ca/climateData/canada_e.html>
- EPA. 2009. *Mobile6 User Guide*, Environmental Protection Agency. United State Environmental Protection Agency: United States. Accessed in July 2009 <<http://www.epa.gov/otaq/models/mobile6/420r03010.pdf>>
- Foken T. 2008. The energy balance closure problem: an overview. *Ecological Applications* **18**(6): 1351–1367.
- Fortuniak K. 2008. Numerical estimation of the effective albedo of an urban canyon. *Theoretical and Applied Climatology* **91**(1–4): 245–258.
- Grimmond CSB. 1992. The suburban energy-balance – methodological considerations and results for a midlatitude westcoast city under winter and spring conditions. *International Journal of Climatology* **12**(5): 481–497.
- Hamilton IG, Davies M, Steadman P, Stone A, Ridley I, Evans S. 2009. The significance of the anthropogenic heat emissions of London's buildings: a comparison against captured shortwave solar radiation. *Building and Environment* **44**(4): 807–817.
- Ichinose T, Shimodozono K, Hanaki K. 1999. Impact of anthropogenic heat on urban climate in Tokyo. *Atmospheric Environment* **33**(24–25): 3897–3909.
- Klysik K. 1996. Spatial and seasonal distribution of anthropogenic heat emissions in Lodz, Poland. *Atmospheric Environment* **30**(20): 3397–3404.
- Kondo A, Ueno M, Kaga A, Yamaguchi K. 2001. The influence of urban canopy configuration on urban albedo. *Boundary-Layer Meteorology* **100**(2): 225–242.
- Lemonsu A, Belair S, Mailhot J, Benjamin M, Chagnon F, Morneau G, Harvey B, Voogt J, Jean M. 2008. Overview and first results of the Montreal urban snow experiment 2005. *Journal of Applied Meteorology and Climatology* **47**(1): 59–75, DOI: 10.1175/2007jamc1639.1.
- Leroyer S, Mailhot J, Belair S, Lemonsu A, Strachan IB. 2010. Modeling the surface energy budget during the thawing period of the 2006 Montreal urban snow experiment. *Journal of Applied Meteorology and Climatology* **49**(1): 68–84, DOI: 10.1175/2009jamc2153.1.
- Masson V. 2000. A physically-based scheme for the urban energy budget in atmospheric models. *Boundary-Layer Meteorology* **94**(3): 357–397.
- Monteith JL, Unsworth MH. 1990. *Principles of Environmental Physics*, Edward Arnold: London, New York.
- Noilhan J, Planton S. 1989. A simple parameterization of land surface processes for meteorological models. *Monthly Weather Review* **117**(3): 536–549.
- Noriega Y, Florian M, Morneau G. 2006. *Computing Mobile Emissions for the Montreal Area*. Centre de Recherche en Transport: Montréal, 10.
- OEE. 2010. *Comprehensive Energy Use Database*, Office of Energy Efficiency. Natural Resource Canada. Accessed in March 2010 <<http://oeo.nrcan.gc.ca/corporate/statistics/neud/dpa/comprehensive-tables/index.cfm?attr=0>>
- Offerle B, Grimmond CSB, Fortuniak K. 2005. Heat storage and anthropogenic heat flux in relation to the energy balance of a central European city centre. *International Journal of Climatology* **25**(10): 1405–1419.
- Offerle B, Grimmond CSB, Fortuniak K, Klysik K, Oke TR. 2006. Temporal variations in heat fluxes over a central European city centre. *Theoretical and Applied Climatology* **84**(1–3): 103–115.

- Oke TR. 1997. Urban environments. In *The surface climates of Canada*, Bailey WG, Oke TR, Rouse WR (eds). McGill-Queen's University Press: Montreal.
- Oke TR. 2006. Towards better scientific communication in urban climate. *Theoretical and Applied Climatology* **84**(1–3): 179–190, DOI: 10.1007/s00704-005-0153-0.
- Pigeon G, Legain D, Durand P, Masson V. 2007. Anthropogenic heat release in an old European agglomeration (Toulouse, France). *International Journal of Climatology* **27**(14): 1969–1981.
- Pigeon G, Moscicki MA, Voogt JA, Masson V. 2008. Simulation of fall and winter surface energy balance over a dense urban area using the TEB scheme. *Meteorology and Atmospheric Physics* **102**(3–4): 159–171.
- Ruffieux D. 1995. Winter surface-energy budget in Denver, Colorado. *Atmospheric Environment* **29**(13): 1579–1587.
- Sailor DJ, Lu L. 2004. A top-down methodology for developing diurnal and seasonal anthropogenic heating profiles for urban areas. *Atmospheric Environment* **38**(17): 2737–2748.
- Sailor DJ, Rosen JN, Munoz JR. 1998. Natural gas consumption and climate: a comprehensive set of predictive state-level models for the United States. *Energy* **23**(2): 91–103.
- Sailor DJ, Vasireddy C. 2006. Correcting aggregate energy consumption data to account for variability in local weather. *Environmental Modelling & Software* **21**(5): 733–738.
- Spronken-Smith RA. 2002. Comparison of summer- and winter-time suburban energy fluxes in Christchurch, New Zealand. *International Journal of Climatology* **22**(8): 979–992, DOI:10.1002/joc.767.
- Spronken-Smith RA, Kossmann M, Zawar-Reza P. 2006. Where does all the energy go? Surface energy partitioning in suburban Christchurch under stable wintertime conditions. *Theoretical and Applied Climatology* **84**(1–3): 137–149.
- Taha H. 1997. Urban climates and heat islands: Albedo, evapotranspiration, and anthropogenic heat. *Energy and Buildings* **25**(2): 99–103.
- Tanner CB, Thurtell GW. 1969. *Anemoclinometer Measurements of Reynolds Stress and Heat Transport in the Atmospheric Surface Layer*, US Army Electronics Command Technical Report No ECOM-66-G22F, University of Wisconsin: Madison, WI, 10.
- Vesala T, Jarvi L, Launiainen S, Sogachev A, Rannik U, Mamarella I, Siivola E, Keronen P, Rinne J, Riikkonen A, Nikinmaa E. 2008. Surface-atmosphere interactions over complex urban terrain in Helsinki, Finland. *Tellus Series B-Chemical and Physical Meteorology* **60**(2): 188–199.
- Vickers D, Mahrt L. 1997. Quality control and flux sampling problems for tower and aircraft data. *Journal of Atmospheric and Oceanic Technology* **14**(3): 512–526.
- Ville de Montréal. 2009a. Population. Montréal en statistiques. Ville de Montréal. Accessed in August 2009. <http://ville.montreal.qc.ca/portal/page?_pageid=2077,2455180&_dad=portal&_schema=PORTAL>
- Ville de Montréal. 2009b. *Discover the City's Large Parks*. Network of large parks. Ville de Montréal. Accessed in August 2009. <http://ville.montreal.qc.ca/portal/page?_pageid=175,4782055&_dad=portal&_schema=PORTAL>
- Webb EK, Pearman GI, Leuning R. 1980. Correction of flux measurements for density effects due to heat and water-vapor transfer. *Quarterly Journal of the Royal Meteorological Society* **106**(447): 85–100.
- Wilson K, Goldstein A, Falge E, Aubinet M, Baldocchi D, Berbigier P, Bernhofer C, Ceulemans R, Dolman H, Field C, Grelle A, Ibrom A, Law BE, Kowalski A, Meyers T, Moncrieff J, Monson R, Oechel W, Tenhunen J, Valentini R, Verma S. 2002. Energy balance closure at FLUXNET sites. *Agricultural and Forest Meteorology* **113**(1–4): 223–243, DOI: Pii S0168-1923(02)00109-0.
- Yao RM, Steemers K. 2005. A method of formulating energy load profile for domestic buildings in the UK. *Energy and Buildings* **37**(6): 663–671, DOI: 10.1016/j.enbuild.2004.09.007.
- Zar JH. 1984. *Biostatistical Analysis*, Prentice-Hall Inc.: Englewood Cliffs, NJ.